JOURNAL OF GEOPHYSICAL RESEARCH, VOL. 113, A01214, doi:10.1029/2007JA012626, 2008

Plasmoids in Saturn's magnetotail

T. W. Hill,[1] M. F. Thomsen,[2] M. G. Henderson,[2] R. L. Tokar,[2] A. J. Coates,[3] H. J. McAndrews,[2] G. R. Lewis,[3] D. G. Mitchell,[4] C. M. Jackman,[5] C. T. Russell,[6] M. K. Dougherty,[5] F. J. Crary,[7] and D. T. Young[7]

Received 3 July 2007; revised 14 September 2007; accepted 10 October 2007; published 26 January 2008.

[1] Plasmoids in Saturn's magnetotail are identified by a reversal (northward turning) of the normally southward component of the magnetic field across the tail current sheet. Three large plasmoids have been identified by the Cassini magnetometer, one near 0300 local time at a planet-centered distance of 44 R_S and two near midnight at 48–49 R_S. ($R_S \approx 60{,}300$ km is Saturn's equatorial radius.) Two of these events, including in particular the 0300 event, coincided with current-sheet crossings by the spacecraft and thus provided sufficient plasma fluxes to determine ion composition and velocity moments from Cassini Plasma Spectrometer data. The composition was largely dominated by water-group ions, indicating an inner-magnetosphere source. The flow was subcorotational and strongly tailward, as expected for a plasmoid. Just before the in situ detection of the 0300 plasmoid, the Magnetospheric Imaging Instrument observed an outburst of energetic neutral atoms emanating from a location midway between Saturn and Cassini, probably a signature of the reconnection event that spawned the plasmoid.

Citation: Hill, T. W., et al. (2008), Plasmoids in Saturn's magnetotail, *J. Geophys. Res.*, *113*, A01214, doi:10.1029/2007JA012626.

1. Introduction

[2] A plasmoid is a transient magnetic loop structure formed by time-dependent magnetic reconnection in a planetary magnetotail. It provides a mechanism for removing plasma from the magnetosphere while conserving magnetic flux. The magnetic flux and the plasma generally move together according to the ideal MHD condition $\mathbf{E} + \mathbf{v} \times \mathbf{B} = 0$. This condition is violated in a microscopic but finite neighborhood of a reconnection line ($\times$ line), allowing the magnetic field topology to change and the plasma to escape from "closed" magnetospheric field lines (i.e., field lines having both ends attached to the planet).

[3] Plasmoids are ubiquitous in Earth's magnetotail, where they play an important role in magnetospheric substorms [e.g., *Russell and McPherron*, 1973; *Hones*, 1984]. They are also clearly observed in Jupiter's magnetotail [e.g., *Russell et al.*, 1998; *Kronberg et al.*, 2005], where they play an integral part in the formation of a tailward planetary wind [*Vasyliunas*, 1983]. Recently *Jackman et al.* [2007] have identified and characterized three large plasmoids observed in Saturn's magnetotail by the Cassini magnetometer (MAG). In this paper we present and analyze related plasma data from the Cassini Plasma Spectrometer (CAPS) and energetic neutral atom (ENA) images from the Magnetospheric Imaging Instrument (MIMI). The MAG, CAPS, and MIMI instruments are described briefly by *Dougherty et al.* [2005], *Young et al.* [2005], and *Krimigis et al.* [2005], respectively.

[4] During its several 2006 magnetotail excursions, the Cassini spacecraft spent most of its time in the southern tail lobe, not in the plasma sheet that separates the northern and southern lobes, probably because of the expected warping of the plasma sheet as described by *Arridge* [2007] and *Jackman et al.* [2007] and illustrated in Figure 1. Such warping of the magnetotail current sheet is quite familiar and well established at Earth [e.g., *Fairfield*, 1980, and references therein]. The plasma sheet lies close to the (observationally indistinguishable) magnetic and rotational equatorial planes in the region close to the planet, within $\sim$10 R_S, corresponding to $\sim$½ of the typical Chapman-Ferraro distance (the magnetopause distance on the planet-Sun line). Farther out, particularly in the tail, the plasma sheet bends over to follow the solar wind direction, which determines the asymptotic symmetry axis of the tail. The 2006 Cassini magnetotail orbits stayed close to Saturn's equatorial plane, and therefore missed the plasma sheet except for the three fortuitous occasions analyzed here,

[1] Physics and Astronomy Department, Rice University, Houston, Texas, USA.
[2] Los Alamos National Laboratory, Los Alamos, New Mexico, USA.
[3] Mullard Space Science Laboratory, University College London, Surrey, UK.
[4] Johns Hopkins University, Applied Physics Laboratory, Laurel, Maryland, USA.
[5] Blackett Laboratory, Imperial College, London, UK.
[6] Institute of Geophysics, University of California, Los Angeles, California, USA.
[7] Space Science and Engineering, Southwest Research Institute, San Antonio, Texas, USA.

0148-0227/08/2007JA012626$09.00

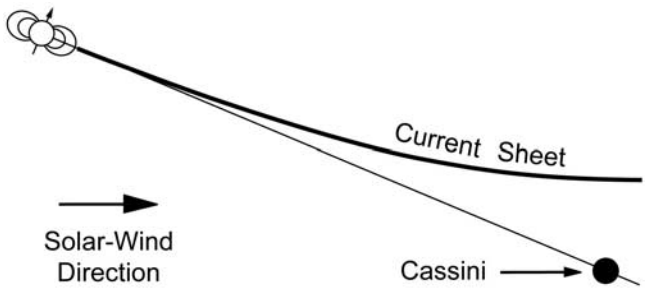

Figure 1. Cartoon illustration of the expected warping of the magnetotail plasma sheet away from Saturn's equatorial plane near the midnight meridian, and hence, unfortunately, away from most of the Cassini 2006 magnetotail orbits.

and a few other plasma sheet encounters (not involving plasmoids) reported recently by *Arridge et al.* [2007].

2. Observations

[5] We adopt the event labels defined in Figure 1 of *Jackman et al.* [2007], whereby plasmoids 1, 2, and 3 occurred respectively on 4 August, 12 July, and 4 March 2006 (inverse chronological order), events 1 and 2 near midnight and event 3 near 0300 local time. We present MAG and CAPS data for events 1 and 3, and MIMI data for event 3.

2.1. Plasmoid 1

[6] Figure 2 shows MAG data (top panel, reproduced with lower time resolution from Figure 2 of *Jackman et al.* [2007]) and CAPS data (remaining panels) for the plasmoid event on 4 August 2006, near midnight at 49 R_S. The second and third panels show, respectively, number densities and temperatures for electrons and two species of positive ions, water-group ions, W^+ (mass 16–18 amu) and protons, H^+. The bottom three panels show the three components of ion flow velocity in the same spin-aligned spherical (r, θ, ϕ) coordinate system as the magnetic field data in the top panel.

[7] The electron moments are obtained by numerical integration of differential fluxes observed by the CAPS Electron Spectrometer (ELS), after removal of spacecraft photoelectrons, under the assumption of isotropy in the spacecraft frame of reference. These are obtained at 2–8 s time resolution for the data shown here, depending on CAPS instrument mode, but have been smoothed with a running average to match the time resolution of the ion moments.

[8] Extraction of ion moments from the CAPS Ion Mass Spectrometer (IMS) is complicated by three factors: (1) intrinsically lower fluxes for ions compared to electrons, (2) the presence of two distinct ion populations, and (3) supersonic flow velocities that often lie outside the CAPS field of view. With respect to point (1), ion data points are shown in the figure only at times for which ion fluxes were sufficiently large and steady to provide reliable ion moments. Each ion data point is obtained from counts accumulated during 14 consecutive instrument cycles (14×32 sec). To deal with point (2) we assumed that the more energetic ion peak is due to water-group ions denoted W^+ (mass between 16 and 18 amu) and that the less energetic peak is due to protons denoted H^+. The two energy peaks are well separated, and their energy ratios are appropriate to this assignment if the speeds are comparable. (The ion fluxes are much too low here to utilize the time-of-flight mass-resolving capability of the IMS. The identification of the higher energy peak as W^+ is always consistent with the time-of-flight analysis when the latter is available.) To overcome difficulty (3), we fit the observed counts in the eight angular sectors to a pair of convecting Maxwellian velocity distributions (one each for W^+ and H^+), with the constraint that the two species share the same flow velocity. This constraint is rigorously true only if the velocity is perpendicular to **B**, which is not true in detail, but relaxing this constraint would result in unequal perpendicular velocities for the two species, which is manifestly implausible. Values for the flow velocity are plotted only for those times when the true flow was clearly in the instrument field of view, as determined by detailed examination of count rates in the eight individual angular sectors (not shown here). The IMS field of view for this interval is shown in Figure A1 of the Appendix. The error bars on the ion moments represent the widths of the minima of the statistical cost function in parameter space.

[9] The MAG data indicate that the B_θ reversal occurred near a true current-sheet crossing, with anticorrelated reversals of B_r and B_ϕ.

[10] The sum of number densities for the two ion species is less than the electron number density by a factor of two or less. This difference is probably attributable to combined measurement and fitting errors, although we cannot rule out the possible admixture of multiply charged ions in the water group. It is interesting to note that the electron temperature is generally closer to the W^+ ion temperature than to the proton temperature, which is opposite to the trend observed in the inner magnetosphere [e.g., *Young et al.*, 2005; *Rymer et al.*, 2007]. This difference can plausibly be attributed to the longer residence time for plasma observed at 49 R_S in the tail, coupled with the longer Coulomb equilibration time for electrons with heavy ions versus protons.

[11] It is unfortunate (but perhaps significant) that ion fluxes became too small for moment extraction just about at the time of the B_θ reversal, announcing the arrival of the center of the plasmoid at Cassini. The electron density drops by a factor ~4 at about this time, possibly indicating the exit of the spacecraft from the central plasma sheet. This could explain the reduction of ion flux, but another possible cause is a deflection of the supersonic ion flow out of the CAPS field of view (see Appendix). Just before the ion signal is lost, there is a clear deflection of ion flow away from the corotation direction (a decrease of v_ϕ) and toward the tailward direction (an increase of v_r). A similar and stronger acceleration is evident in plasmoid 3 (below), for which ion moments are more plentiful.

2.2. Plasmoid 2

[12] This plasmoid, also near midnight but on the previous apoapsis (12 July 2006), did not involve a current sheet crossing, as evidenced by the lack of B_r and B_ϕ reversals [*Jackman et al.*, 2007]. It resembles a "traveling compression region" in Earth's magnetotail [*Siscoe et al.*, 1984] that

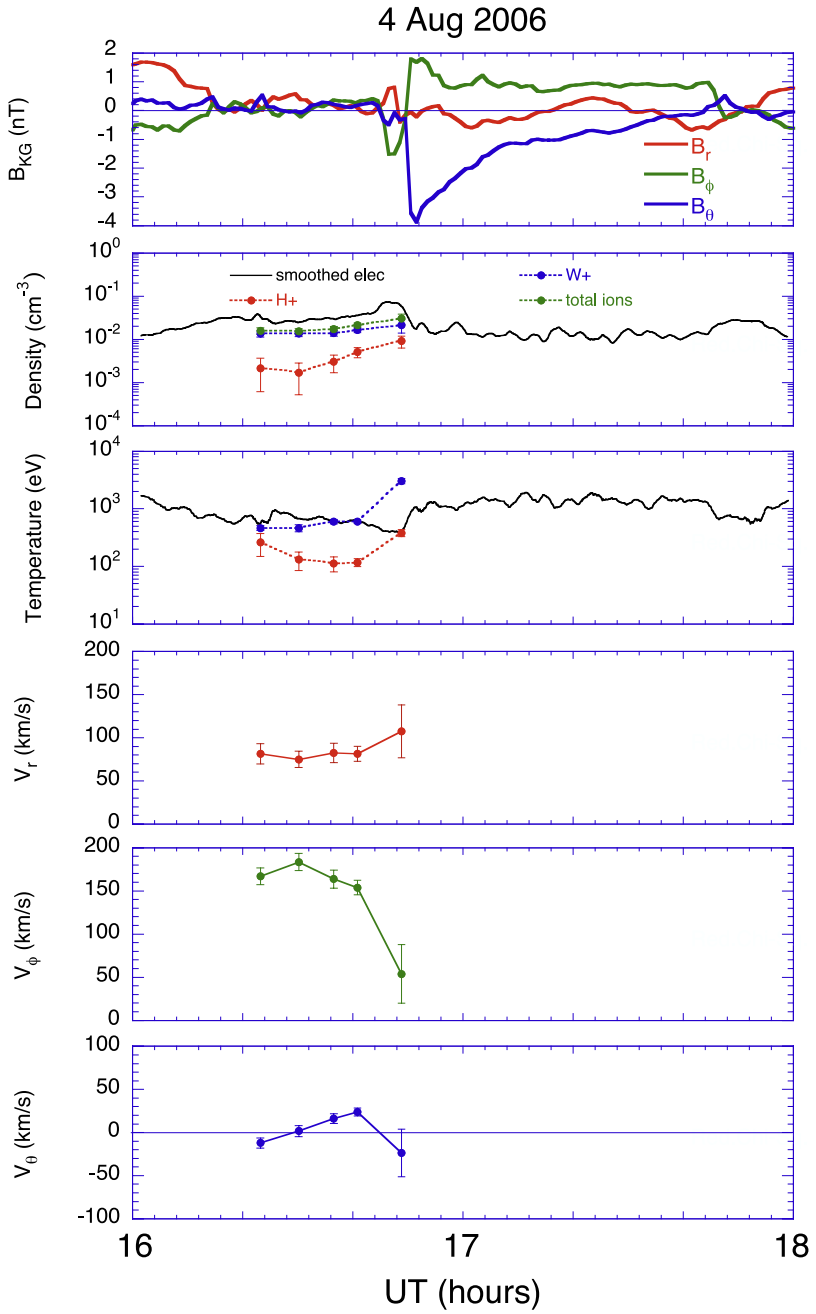

Figure 2. MAG and CAPS data for the plasmoid event on 4 August 2006. Top panel: magnetic field components in a spin-aligned spherical (r, θ, ϕ) coordinate system. Next panel: number densities of electrons, water-group ions W^+, and protons H^+. Next panel: temperatures for the same species. Bottom three panels: ion velocity components in the same (r, θ, ϕ) coordinate system. Rigid corotation would imply v_ϕ = 477 km/s, off the top of the v_ϕ scale.

reflects a near-miss encounter with a tailward-moving plasmoid. Because the central plasma sheet was not encountered, ion fluxes were not sufficient to yield reliable ion moments, so this event is not further discussed here.

2.3. Plasmoid 3

[13] This event, occurring on 4 March 2006 near 0300 local time at a range of 44 R_S, was more amenable to derivation of ion moments. The results are shown in Figure 3, in the same format as Figure 2. There were four notable negative excursions of B_θ, of which the last and largest occurred at about 2300. The preceding hour was characterized by small and variable field components with anticorrelated perturbations of B_r and B_ϕ, indicative of close proximity to the magnetotail current sheet. Correspondingly, the ion fluxes were large enough to provide reliable moments for an extended interval surrounding the plasmoid(s). (For this event the geometry of Figure 1 does not apply–Saturn's equatorial plane, and Cassini, were actually slightly above the ecliptic plane at 0300 local time. Saturn was roughly midway between solstice and equinox.)

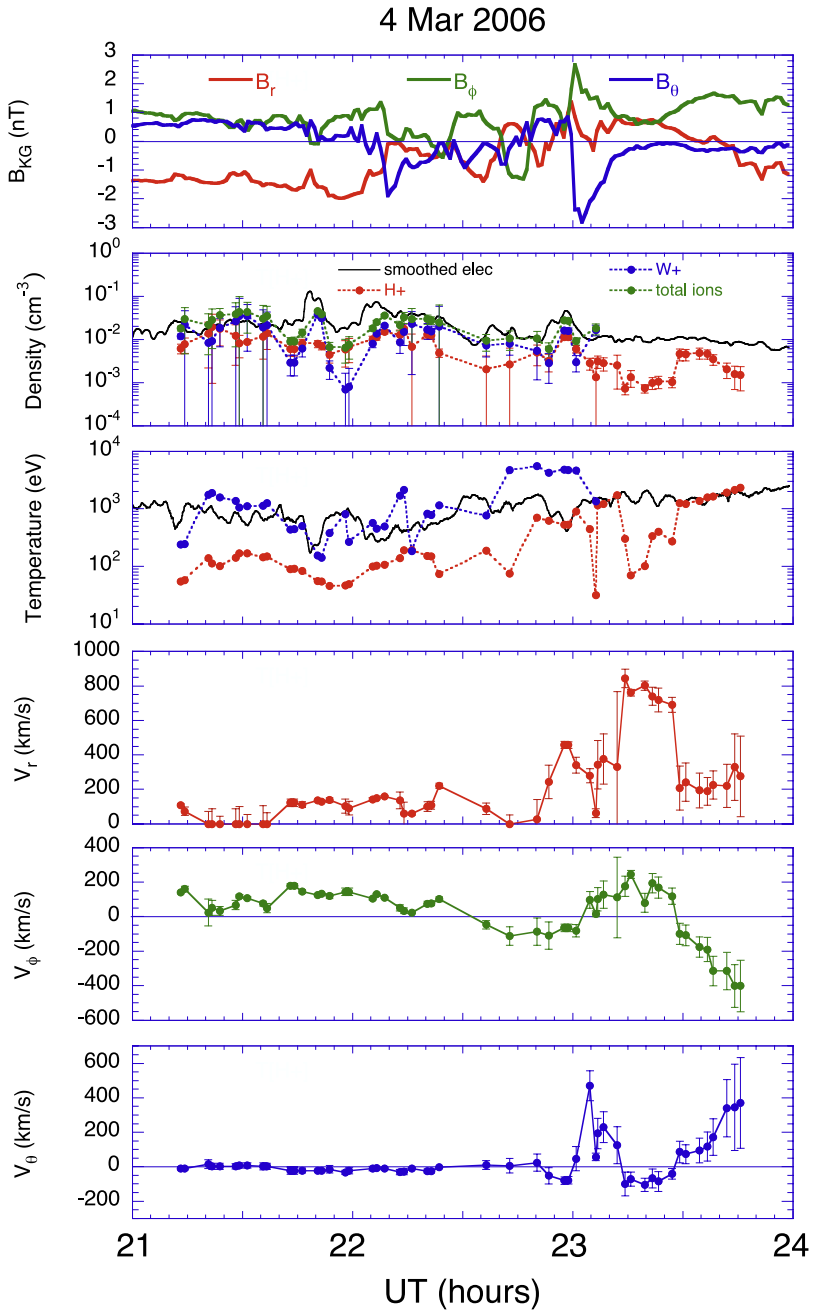

Figure 3. MAG and CAPS data for the plasmoid event on 4 Mar 2006, in the same format as Figure 2. Rigid corotation would imply v_ϕ = 430 km/s, off the top of the v_ϕ scale.

[14] As in the 4 August event, the ion composition was generally (but not always) dominated by W^+. The electron temperature again tracks the W^+ temperature early in the event but fails to keep up with the dramatic increase in the latter after ~2230. Instead, after that time, the electron temperature matches (perhaps by coincidence) the peaks of the rapidly varying proton temperature, which approaches values comparable to the former W^+ temperature. After about 2310 the W^+ energy (mostly flow energy) evidently went off scale above the top of the IMS energy range, 50 keV (this is more evident in the energy-time spectrograms, not shown here), and thereafter the ion velocity moments are based on the proton peak alone.

[15] Also as in the 4 August event, the flow vector generally rotated away from the azimuthal direction and toward the radial direction during the approach of the plasmoid(s), for ~1 h before the largest B_θ reversal at 2300. Note, however, the brief interval around 2245 when the flow was almost entirely in the anticorotation direction. This was followed by a brief interval (~2305–2310) of strongly southward flow (positive v_θ), and a longer period (~ 2315–2330) of extraordinarily fast radial flow along with a strong prograde azimuthal component approaching ½ of rigid corotation (430 km/s at this distance). Toward the end of the plasmoid encounter the flow became generally tailward but with a strong southward component. (At 0300

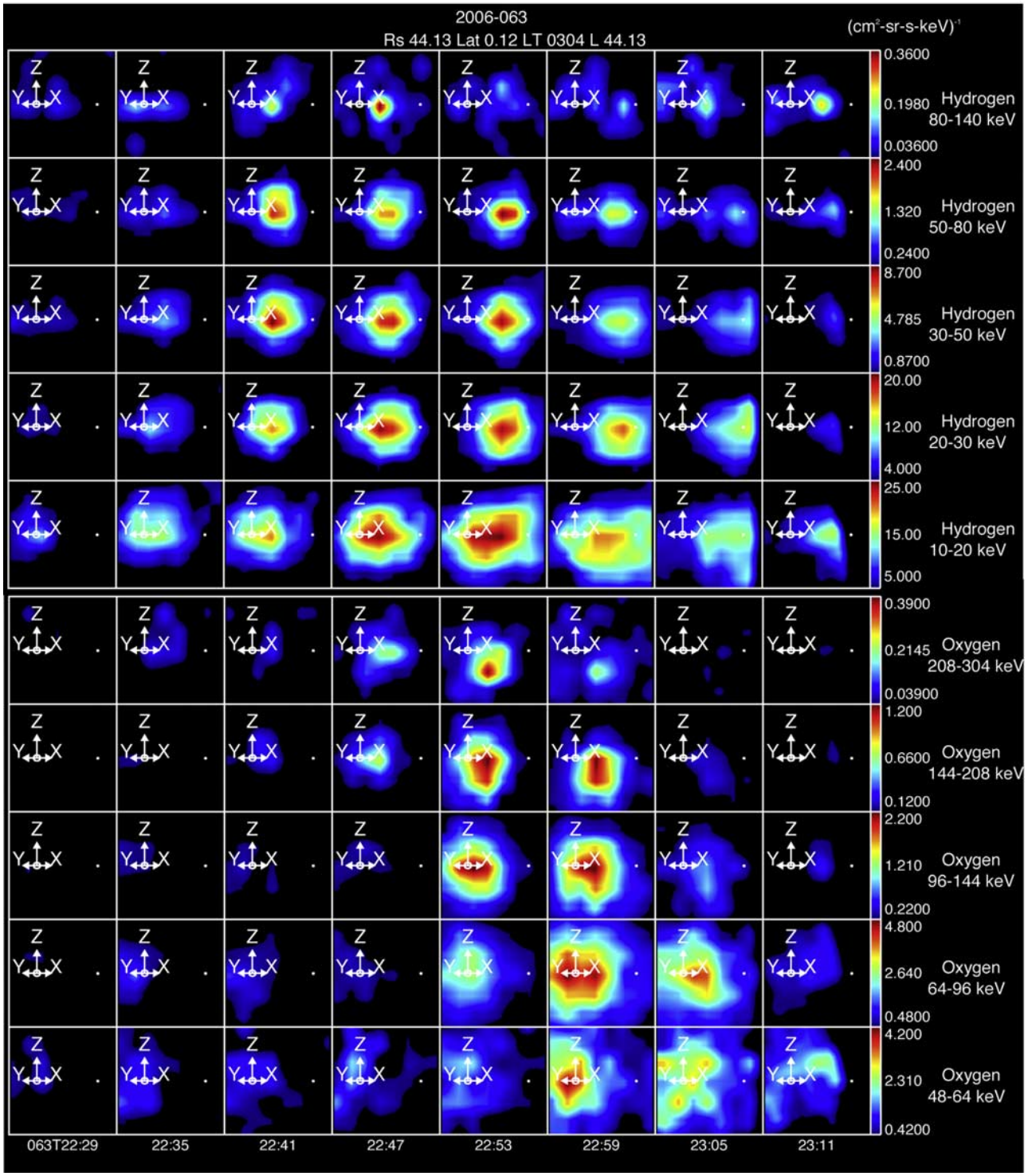

Figure 4. MIMI ENA images for hydrogen (top five rows) and oxygen (bottom five rows) for times ranging from 2229 (left column) to 2311 (right column) on 4 March 2006. Hydrogen energies range from 80–140 keV (top row) down to 10–20 keV (row 5) and oxygen energies range from 208–304 keV (row 6) to 48–64 keV (row 10). The inferred source location is indicated in Figure 5.

local time, a purely antisunward flow would contain approximately equal radial and anticorotational components, roughly consistent with the r and ϕ components observed toward the end of this interval.) Some of the smaller-scale velocity deflections (but probably not the generally tailward rotation) may well result from a temporary mismatch between the planet-centered spherical coordinate system and the true (and undoubtedly fluctuating) orientation of the current sheet. The IMS field of view for this interval is shown in Figure A2 of the Appendix.

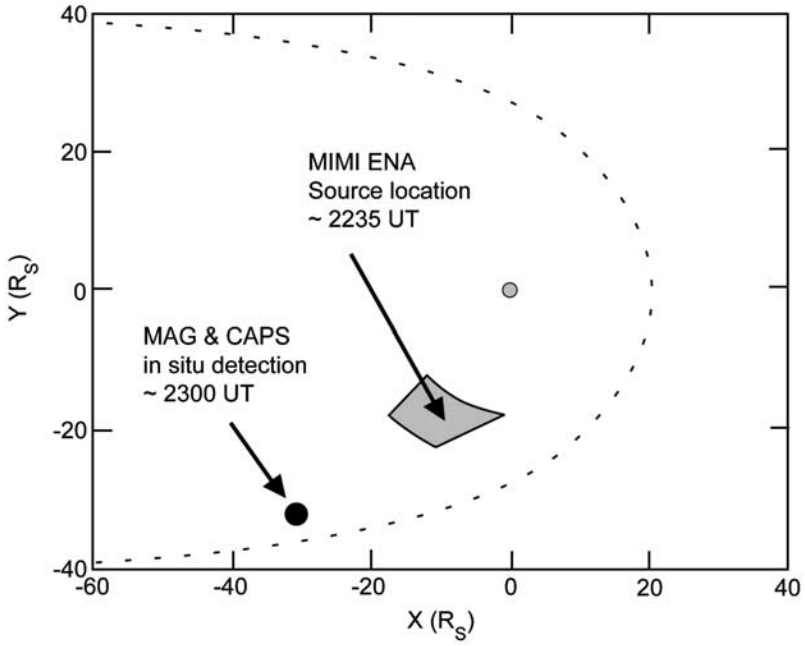

Figure 5. From the observed direction of arrival, coupled with time-of-flight velocity dispersion, the ENA bursts shown in Figure 4 can be inferred to have originated within the shaded box at a time ~25 min before the in situ detection of the large B_θ reversal at Cassini (denoted by the large dot). The view is in Saturn's equatorial plane, and the dashed line is a cartoon illustration of a typical magnetopause location with the Sun to the right.

2.4. ENA Signature of Plasmoid 3

[16] During this event, an intense burst of energetic neutral atoms (ENAs) was detected by the Magnetospheric Imaging Instrument, from a source located between Saturn and Cassini. The relevant ENA image sequence is shown in Figure 4, covering a time interval ranging from 2229 (left column) to 2311 (right column) on 4 March 2006. The top five rows show hydrogen atom flux at energies ranging from 80–140 keV (top row) down to 10–20 keV (row 5). The bottom five rows show oxygen atom flux at energies ranging from 208–304 keV (row 6) down to 48–64 keV (row 10). The peak hydrogen flux arrived at the spacecraft at about 2254 with energies ~10 keV (implying speeds ~1.4 R_S/min), and the peak oxygen flux arrived at about 2259 with energies ~100 keV (implying speeds ~1.1 R_S/min). If we assume that both species started at the same time and the same distance, we can solve uniquely for that time (~2235) and distance (~26.5 R_S).

[17] The inferred source location of these ENA bursts is shown by the shaded box in Figure 5. The left and right sides of this box, as viewed from Cassini, are the viewing directions of the MIMI detector at the first and next-to-last time frames shown in Figure 4, while the near and far sides are the minimum and maximum ranges based on a more careful analysis of the time-of-arrival-versus-velocity dispersion that is evident in Figure 4. The above back-of-envelope estimate falls near the center of this box.

3. Discussion and Conclusions

[18] All three plasmoids identified by *Jackman et al.* [2007] display the classic magnetic signature of terrestrial and Jovian plasmoids, a temporary but persistent reversal of the field component across the magnetotail current sheet. The magnetic signatures alone indicate that Cassini crossed the current sheet during the passages of the 4 March and 4 August plasmoids (cases 3 and 1 respectively) but not during the 12 July event (case 2). Consistent with these signatures, we have found larger plasma densities in events 1 and 3 than in event 2. The larger densities have enabled us to extract ion velocity moments for a short segment of event 1 and a longer portion of event 3. In both cases, especially in case 3, we observe largely azimuthal flow early in the event, rotating to strongly tailward flow as the B_θ reversal (magnetic O line) passes the spacecraft. Before the O line passage, the azimuthal flow was ~10–40% of the rigid corotation speed in event 1, and ~0–50% in case 3. In event 3, where ion moments are available after the O line passage, the total velocity, largely tailward, approached twice the rigid corotation speed.

[19] Thus like the magnetic signatures, the plasma signatures, when available, are consistent with a plasmoid interpretation. They differ, however, from Earth-like substorm plasmoids in two important respects. The ion composition is similar to that in the inner magnetosphere (dominated by W^+ [*Young et al.*, 2005]), and the azimuthal flow component is predominantly prograde in the early portion of the event. These features are qualitatively consistent with the idea of plasmoids produced by a centrifugally driven planetary wind [*Hill et al.*, 1974], as illustrated in Figure 6, reproduced from Figure 11.19 of *Vasyliunas* [1983]. This sketch was originally offered as a description of a possible steady state (or time averaged) configuration in

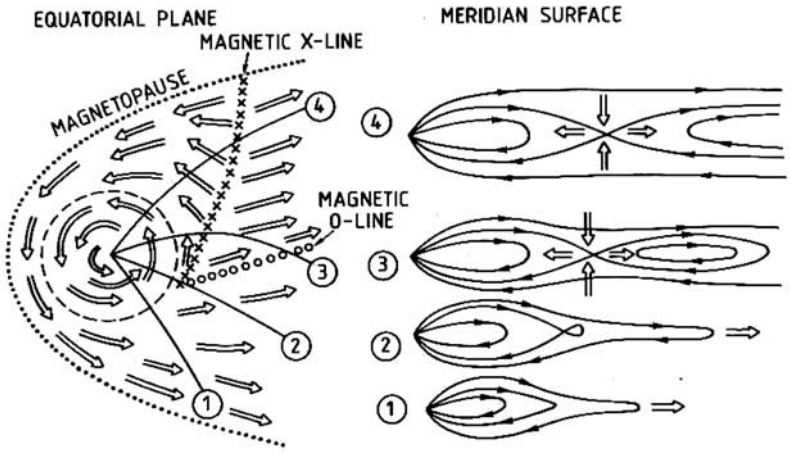

Figure 6. Sketch of a centrifugally driven planetary wind, reproduced from Figure 11.19 of *Vasyliunas* [1983]. The left side shows plasma flow (open arrows) in the equatorial plane and possible locations of steady state magnetic × and O lines. The right side shows resulting magnetic field line configurations in the four meridian surfaces marked on the left. Although the sketch was intended to describe a steady state or time-averaged structure at Jupiter, it provides a useful context for the interpretation of the highly nonsteady plasmoid observations at Saturn.

Jupiter's magnetosphere. The theoretical arguments that motivated it are, however, equally applicable to Saturn.

[20] The plasmoids that we have observed are clearly not steady state structures, but there is nothing in the original arguments of *Vasyliunas* [1983] that requires a steady state structure. A time-dependent version of the same phenomenon has been discussed by *Kivelson and Southwood* [2005] and depicted in their Figure 4b. The formation and motion of a time-dependent plasmoid can be conceptualized as a time variation of the × and O line positions in Figure 6. Alternatively, the sequence 1–4 on the right side of Figure 6 can be read as a time sequence on a given meridian (e.g., 4) rather than a spatial evolution with increasing local time. The qualitative message of Figure 6 is that plasmoid formation is expected to be more prevalent in the midnight-dawn quadrant than in the dusk-midnight quadrant. The midnight-dawn quadrant is, of course, where the three plasmoids described here were found, but Cassini has yet to visit the dusk-midnight quadrant.

[21] The ENA burst shown in Figure 4 can be attributed to sudden plasma heating and acceleration at the newly formed × line that creates the plasmoid and launches it on its tailward motion. (Another necessary ingredient, of course, is a ready supply of neutral charge-exchange partners. The origin of this neutral water-group and hydrogen cloud is outside the scope of this paper, but we note that ENA (O and H) bursts originating from this planet-centered distance are not uncommon [*Mitchell et al.*, 2005].) The inferred location of the ENA source (Figure 5) is considerably Sunward of the expected location of the × line based on a literal interpretation of Figure 6. However, *Vasyliunas* [1983] emphasized that the figure is a free-hand sketch and its details are not to be interpreted literally. There is, unfortunately, no quantitative theoretical model of the planetary wind process with which to compare.

[22] If, as we suggest, the ENA burst signaled the formation of a new magnetic × line, we can estimate the speed of the subsequent plasmoid motion by comparing the time and location of the ENA burst with that of the plasmoid passing the spacecraft. The ENA burst is inferred to have occurred at ~2235 at a location ~26.5 R_S upstream of Cassini. The magnetic O line, which must have started at some intermediate distance, arrived at Cassini at ~2300 (the largest B_θ reversal), implying an upper limit of ~26.5 R_S/25 min ~1000 km/s for its average tailward speed. The arrival of the × line at Cassini is more difficult to pinpoint, but probably occurred around 2325, when B_θ returned to a value near zero (Figure 3). (The subsequent half hour when B_θ lingers at slightly negative values may result from a small mismatch between the idealized equatorial plane of the (r, θ, ϕ) coordinate system and the actual current-sheet symmetry surface, as suggested by the fact that B_r and B_ϕ are not well anticorrelated after the O line passage.) This would suggest an average × line speed of ~26.5 R_S/50 min ~500 km/s, or half of the upper limit estimated above for the O line speed.

[23] These speed estimates are not definitive but they are plausible. For example, the maximum measured ion flow speed in this plasmoid, largely tailward, was ~800 km/s relative to Saturn (Figure 3), comparable to our inferred upper limit on the average O line speed. The O line is expected to move at the local plasma velocity in the plane perpendicular to the O line because the $\mathbf{E} \times \mathbf{B}$ flow is toward the O line from all sides in that plane [*Vasyliunas*, 1980, 1983]. Our measured ion flow and inferred O-line velocity are consistent with this expectation.

[24] It is obvious that no general conclusions can be drawn on the basis of only three events, of which only two allowed a determination of plasma flow velocity. All that can be said is that these three events displayed signa-

tures that are consistent with the plasmoid picture, and there is no other theoretical picture available to explain them. No estimate of occurrence frequency is possible because of the unfavorable observing geometry shown in Figure 1. (A lower limit of one event per month is justified, but is probably very much smaller than the real occurrence frequency.) There is some hope of additional magnetotail orbits during an extended Cassini mission, and if so, the geometry near midnight should be more favorable than indicated in Figure 1 because Saturn would be near its August 2009 equinox.

Appendix

[25] The CAPS IMS instrument includes eight nominally identical detectors arrayed in a planar fan spanning 160° of the instrument-centered polar angle θ ($10° < \theta < 170°$), 20° per detector. When the actuator is operating, as it was for the observations presented here, this fan is swept perpendicular to itself through an azimuthal range of ≈165° every ≈3 min (full period ≈6.25 min), providing a field of view $\sim 2\pi$ steradians. (Cassini is a three-axis-stabilized spacecraft.) The resulting field of view is illustrated in Figure A1 for a representative time during the plasmoid #1 event on 4 August 2006, and in Figure A2 for two representative times (before and after a spacecraft roll maneuver) during the plasmoid #3 event on 4 March 2006.

[26] Each figure shows the celestial sphere as viewed from Cassini looking toward Saturn (the dot at the center of the figure). The linear radial coordinate from this dot is the angular difference from the Saturn direction, equal to 90° on the dashed white circle and 180° on the solid white circle (which therefore maps to a single point, the anti-Saturn point, on the unit sphere). The angular coordinate on these polar plots is azimuthal angle measured relative to the projection of Saturn's spin axis, not shown but oriented vertically upward in each figure. Each IMS detector is represented by a differently colored swath (dark blue= detector 1, red=detector 8). The corotation direction is represented by a yellow arrowhead (which falls, by definition, on the dashed white 90° circle), and the computed ion flow velocity is represented by a purple arrowhead.

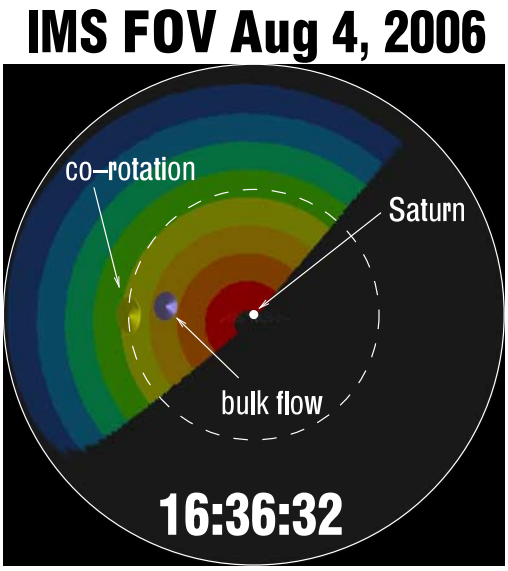

Figure A1. CAPS IMS field of view for the observation interval of Figure 2.

[27] Note that both the Saturn direction and the computed flow direction lie within the IMS field of view during these observations. The corotation direction also lies in the field of view for the 4 August interval, and for most but not all of the 4 March interval.

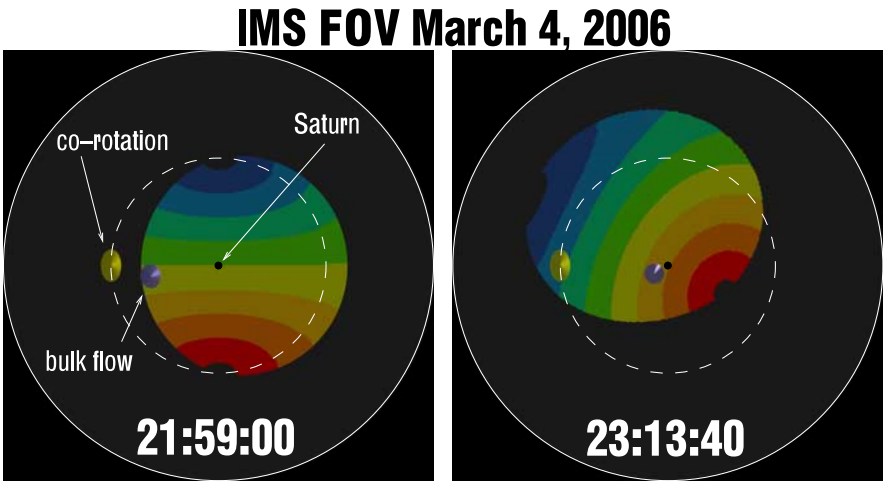

Figure A2. CAPS IMS field of view for the observation interval of Figure 3, before and after a spacecraft roll maneuver.

[28] **Acknowledgments.** We thank V. M. Vasyliunas and both reviewers for their helpful comments. Work at Rice and SWRI was supported by NASA JPL contract 1243218 to SWRI. Work at LANL was supported by the U.S. Department of Energy. Work at IC and MSSL was supported by the Science and Technology Facilities Council. Work at JHU/APL was supported by NASA OSS contract NAS5-97271. Work at UCLA was supported by NASA JPL contract 1236948.

[29] Wolfgang Baumjohann thanks Vytenis M. Vasyliunas and another reviewer for their assistance in evaluating this paper.

References

Arridge, C. S. (2007), On the configuration and dynamics of Saturn's magnetosphere, Ph.D. thesis, Imperial College, London.

Arridge, C. S., et al. (2007), Plasma electrons in Saturn's magnetotail, presented at Magnetospheres of the Outer Planets conference, San Antonio, TX, June 25–29.

Dougherty, M. K., et al. (2005), Cassini magnetometer observations during Saturn orbit insertion, *Science*, *307*, 1266.

Fairfield, D. H. (1980), A statistical determination of the shape and position of the geomagnetic neutral sheet, *J. Geophys. Res.*, *85*, 775.

Hill, T. W., A. J. Dessler, and F. C. Michel (1974), Configuration of the jovian magnetosphere, *Geophys. Res. Lett.*, *1*, 3.

Hones, E. W., Jr. (1984), Plasma sheet behavior during substorms, in *Magnetic Reconnection in Space and Laboratory Plasmas*, *AGU Geophys. Monograph Ser.*, Vol. 30, edited by E. W. Hones Jr., p. 178, AGU, Washington, D. C.

Jackman, C. M., C. T. Russell, D. J. Southwood, C. S. Arridge, N. Achilleos, and M. K. Dougherty (2007), Strong rapid dipolarizations in Saturn's magnetotail: In situ evidence of reconnection, *Geophys. Res. Lett.*, *34*, L11203, doi:10.1029/2007GL029764.

Kivelson, M. G., and D. J. Southwood (2005), Dynamical consequences of two modes of centrifugal instability in Jupiter's outer magnetosphere, *J. Geophys. Res.*, *110*, A12209, doi:10.1029/2005JA011176.

Krimigis, S. M., et al. (2005), Dynamics of Saturn's magnetosphere from MIMI during Cassini's orbital insertion, *Science*, *307*, 1270.

Kronberg, E. A., J. Woch, N. Krupp, A. Lagg, K. K. Khurana, and K.-H. Glassmeier (2005), Mass release at Jupiter: Substorm-like processes in the Jovian magnetotail, *J. Geophys. Res.*, *110*, A03211, doi:10.1029/2004JA010777.

Mitchell, D.G., et al. (2005), Energetic ion acceleration in Saturn's magnetotail: Substorms at Saturn?, *Geophys. Res. Lett.*, *32*, L20S01, doi:10.1029/2005GL022647.

Russell, C. T., and R. L. McPherron (1973), The magnetotail and substorms, *Space Sci. Rev.*, *15*, 205.

Russell, C. T., K. K. Khurana, D. E. Huddleston, and M. G. Kivelson (1998), Localized reconnection in the near Jovian magnetotail, *Science*, *280*, 1061.

Rymer, A. M., et al. (2007), Electron sources in Saturn's magnetosphere, *J. Geophys. Res.*, *112*, A02201, doi:10.1029/2006JA012017.

Siscoe, G. L., D. G. Sibeck, J. A. Slavin, E. J. Smith, B. T. Tsurutani, and D. E. Jones (1984), ISEE 3 magnetic field observations in the magnetotail: implications for reconnection, in *Magnetic Reconnection in Space and Laboratory Plasmas*, *AGU Geophys. Monograph Ser.*, Vol. 30, edited by E. W. Hones Jr., p. 240, AGU, Washington, D. C.

Vasyliunas, V. M. (1980), Upper limit on the electric field along a magnetic O line, *J. Geophys. Res.*, *85*, 4616.

Vasyliunas, V. M. (1983), Plasma distribution and flow, in *Physics of the Jovian Magnetosphere*, edited by A. J. Dessler, chap. 11, p. 395, Cambridge Univ. Press, New York.

Young, D. T., et al. (2005), Composition and dynamics of plasma in Saturn's magnetosphere, *Science*, *307*, 1262.

A. J. Coates and G. R. Lewis, Mullard Space Science Laboratory, University College London, Surrey, UK.

F. J. Crary and D. T. Young, Space Science and Engineering, Southwest Research Institute, San Antonio, TX, USA.

M. K. Dougherty and C. M. Jackman, Blackett Laboratory, Imperial College, London, UK.

M. G. Henderson, H. J. McAndrews, M. F. Thomsen, and R. L. Tokar, Los Alamos National Laboratory, Los Alamos, NM, USA.

T. W. Hill, Physics and Astronomy Department, Rice University, BOX 1892, MS 108 6100 S. Main, Houston, TX, USA. (hill@rice.edu)

D. G. Mitchell, Johns Hopkins University, Applied Physics Laboratory, Laurel, MD, USA.

C. T. Russell, Institute of Geophysics, University of California, Los Angeles, CA, USA.